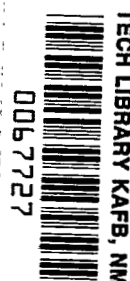


**NASA
Technical
Paper
2156**

May 1983

NASA
TP
2156
c.1



Particle Sizing by Measurement of Forward-Scattered Light at Two Angles

Donald R. Buchele

LOAN COPY: RETURN TO
AFWL TECHNICAL LIBRARY
KIRTLAND AFB, N.M.

NASA



25th Anniversary
1958-1983

posted 2/6/84

ERRATA

NASA Technical Paper 2156

PARTICLE SIZING BY MEASUREMENT OF FORWARD-
SCATTERED LIGHT AT TWO ANGLES

Donald R. Buchele
May 1983

Page 7, first paragraph, lines 5 and 6: The numbers 10 10 should be replaced by $10\sqrt{10}$.

Page 15, third line from bottom: The reference number should be 7 instead of 4.

Page 19, second paragraph from bottom, line 1: The symbol should be B' instead of B_1 .



Particle Sizing by Measurement of Forward-Scattered Light at Two Angles

Donald R. Buchele
*Lewis Research Center
Cleveland, Ohio*



National Aeronautics
and Space Administration

Scientific and Technical
Information Branch

SUMMARY

Forward-scattered light can provide a measure of particle diameter when the diameter is much greater than the wavelength of radiation. The light scattered by one or more particles in a test section was shown by experiment and analysis to be affected by extraneous light from a number of sources. Methods of minimizing the extraneous light are presented for application to instrument design. Two types of instrument are described and compared.

INTRODUCTION

The performance and pollutant emission of a gas turbine combustor is significantly dependent on the diameter of the fuel particles sprayed from the fuel nozzle. When the particle diameter is much greater than the wavelength of radiation, the diameter can be inferred from the angular distribution of light scattered in the forward direction from a narrow, collimated beam.

Reference 1 shows that a useful measure of particle diameter is derivable from the shape of the center lobe of the intensity distribution of forward-scattered radiation. The intensity may be calculated by the Fraunhofer diffraction formula instead of the more exact Mie formula. Although there is a substantial discrepancy between the two formulas in the calculation of absolute intensity when the particle diameter approaches the wavelength of radiation, the absolute value of intensity can be eliminated by measuring the ratio of intensities at two fixed scattering angles. The lower limit of measurable particle diameter then becomes of the order of the wavelength of the radiation. The upper limit of measurable particle diameter is set by the increasing difficulty of measuring intensities as the angular width of the center lobe becomes smaller for a larger diameter. The method was studied in reference 2, and an instrument was built (ref. 3) that measures single particles. Forward scattering in the center lobe is shown in references 4 to 6 to determine the Sauter mean diameter of a polydispersion of particles.

Another method (ref. 7) to be considered measures the angles, one fixed and one variable, where there exists a fixed ratio of two intensities. Both methods are compared herein for application to instrument design. The analysis will assume monochromatic radiation, since, in present-day practice, a laser is invariably chosen as the radiation source. The particle-diameter range of particular interest is 10 to 100 micrometers. The following measurement errors will be considered, together with techniques of reducing the magnitude of the error:

(1) Light diffracted by the test section aperture undesirably adds to the light scattered by the particles themselves. This undesirable light can be intercepted by spatial filters or reduced by apodization.

(2) A coherent laser source produces interference of scattered light and thus superimposes speckle on the intensity pattern that is measured. Integration, either temporal or spatial, can reduce this effect on the measurement.

(3) Refraction by turbulent gas in the test section can broaden the image of a point source. This problem can be treated by the same techniques that are used to correct for a source of larger diameter.

(4) Error of intensity measurement results in particle sizing error even when one measures the ratio of intensities at two angles of measurement. The selection of optimum angles can reduce the resultant error.

(5) Some error is introduced by neglecting processes other than Fraunhofer diffraction. These additional processes are included in the analysis by Mie. An indication will be given of the magnitudes of the differences between the two treatments.

SYMBOLS

A	test section aperture
A'	image of A
B	image plane at focal length f (fig. 4(a))
B'	image of B
C	$0.57\pi/\lambda$
D	diameter of particle or aperture
D_{32}	Sauter mean diameter of particles
F_1, F_2	error ratio factors
f	focal length of objective lens (fig. 1)
G	intensity gain factor with many particles
H	irradiance
I	light intensity
J_1	first-order Bessel function
K	scattering coefficient of one particle
N	number of particles
P	radiant power
y	ray displacement at focal length f (fig. 1)
α	particle size parameter, $\pi D/\lambda$
δA	detector area (fig. 1)
θ	ray deviation angle at focal length f (fig. 1)
λ	wavelength of radiation
τ	transmission factor of particles

Subscripts:

b	light beam
h	vertical axis of ellipse
p	particle
w	horizontal axis of ellipse
0	at angle $\theta = 0$
1/2	at half of maximum amplitude
1	at smaller angle θ of measurement
2	at larger angle θ of measurement
3	angle measured by scanning system (eq. (16))

SCATTERING ANALYSIS

Angular Distribution of Forward Scattered Light

An optical system (described in refs. 4 and 8) for measuring the radiant flux at any small angle of forward scattering is shown in figure 1. Light from a point source is collimated by a lens, passes through the test section, and is then focused to a point in the focal plane by an objective lens. Light scattered anywhere in the test section at an angle θ intersects the focal plane at a distance y from the focal point. Thus,

$$\theta = \frac{y}{f} \quad (1)$$

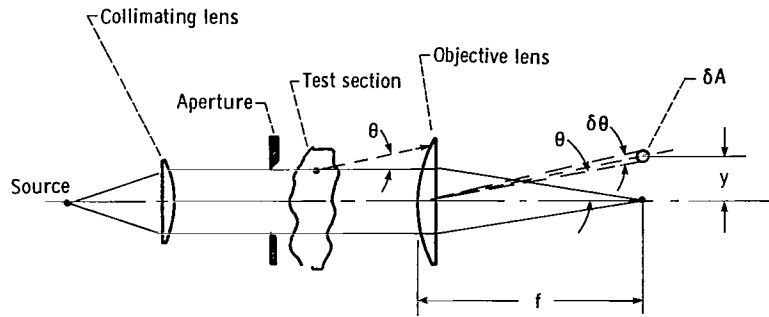


Figure 1. - Optical system.

for $y/f \ll 1$, where f is the lens focal length. At the focal plane, a detector with area δA subtends a cone with apex at the lens and with its axis in direction θ . The radiant power received by the area δA determines the irradiance as $H = P/\delta A$, power/area. The intensity in direction θ is $I = Pf^2/\delta A$, power/steradian. Thus, the intensity and irradiance are related by only a constant as

$$H = \frac{I}{f^2} \quad (2)$$

This conversion is useful when calculating the power available to a detector at a given intensity.

When measuring particles larger than 10 micrometers in diameter, the light in the center lobe is due principally to Fraunhofer diffraction rather than to the additional processes of reflection and absorption that are included in Mie's analysis.

Useful approximations for the intensity distribution of forward-scattered light in the center lobe (the lobe with maximum intensity at $\theta = 0$) are plotted in figure 2. The ordinate is the intensity at a scattering angle θ divided by the intensity at $\theta = 0$, the direction of the incident light. The abscissa is a beam-spread parameter $\alpha\theta$ where the particle size parameter is

$$\alpha = \frac{\pi D}{\lambda} \quad (3)$$

with particle diameter D and wavelength λ .

The curve for a monodispersion is given by Fraunhofer diffraction (ref. 1) as

$$\frac{I(\theta)}{I(0)} = \left[\frac{2J_1(\alpha \sin \theta)}{\alpha \sin \theta} \right]^2 \quad (4)$$

where J_1 is the first-order Bessel function. For $\theta < 20^\circ$, $\sin \theta$ may be replaced by θ in radians.

The two curves for a polydispersion of particles are based on the Sauter mean diameter D_{32} . This diameter is the ratio of total particle volume to total particle surface area. The curves were derived in references 4 and 5 using the monodisperse function with a wide variety of particle-diameter distributions in which no particles exist with a diameter larger than approximately ten times the Sauter mean diameter.

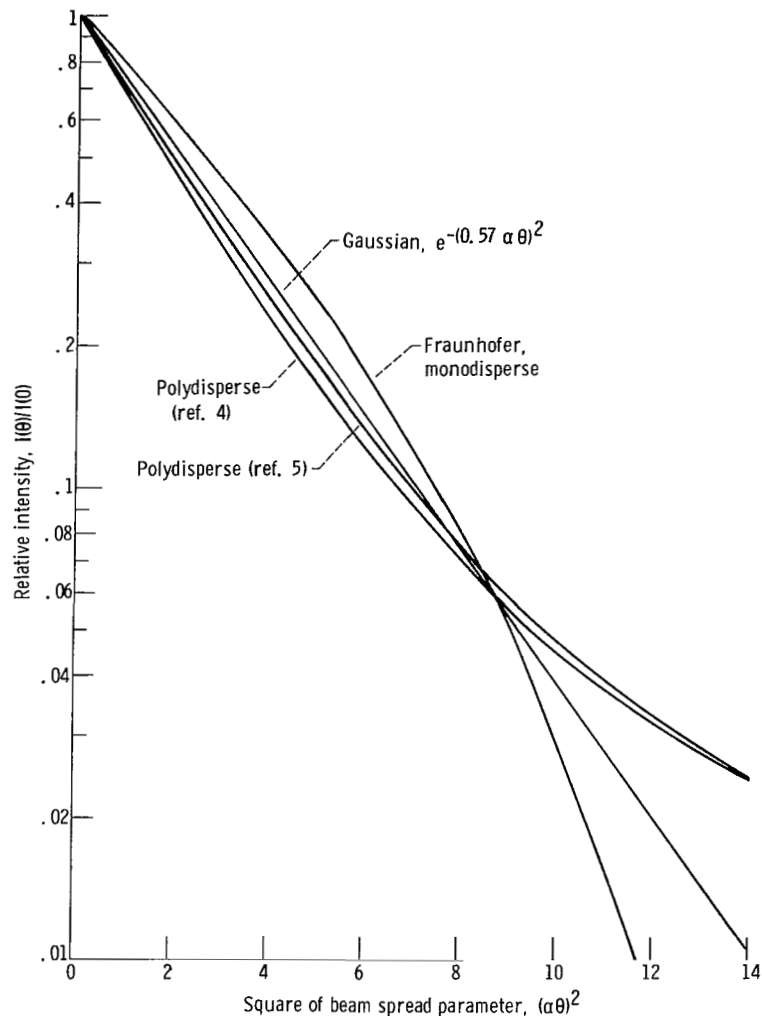


Figure 2. - Distribution of forward-scattered light. (Ray deviation angle θ in radians.)

The Gaussian curve is a good approximation to the other curves, and it is a good approximation to the curve found in reference 6 to best represent the intensity distribution of light scattered by fuel spray. At $\alpha\theta > 3$, all curves in figure 2 agree with each other within 5 percent of full scale.

Diffraction by Test-Section Aperture

The intensity distribution described by the Fraunhofer diffraction equation (4) applies both to the spray particles and to the test-section aperture. The diffraction by the aperture is often ignored or not realized to exist. The test methods used in references 9 and 10 eliminate the effects of diffraction by the aperture as well as the effects of other sources of interfering light.

Because the test-section aperture diameter is much greater than a particle diameter, the aperture produces more scattered flux than a small number of particles. This flux has a strong effect on the resultant intensity distribution as measured.

The Fraunhofer equation gives the intensity as

$$I(\theta) = \frac{H\lambda^2}{16\pi^2} \left[\frac{2J_1(\alpha\theta)}{\alpha\theta} \right]^2 \quad (5)$$

where H is the irradiance of a plane wave of radiation at the aperture.

The Bessel function J_1 has peak values, the first one beginning at $\alpha\theta = 1.84$, that are closely approximated by an asymptotic formula (ref. 11):

$$J_1(\alpha\theta) = (2/\pi\alpha\theta)^{1/2} \cos(\alpha\theta - 3\pi/4) \quad (6)$$

Equation (6), with the cosine factor replaced by unity (its maximum possible value), is substituted in equation (5) to yield an approximate envelope of the intensity peaks for $\alpha\theta > 1.84$. Along this envelope, for $\alpha\theta \geq 1.84$,

$$I(\theta) = \left(\frac{H\lambda^2}{16\pi^2} \right) \left(\frac{8\alpha}{\pi\theta^3} \right) \quad (7)$$

Figure 3 shows a relative intensity $I(\theta, D)/I(0, D_0)$ for a circular aperture or circular particle as a function of angle θ and diameter D ($D_0 = 10\,000\ \mu\text{m}$, $\lambda = 1\ \mu\text{m}$). For clarity, the intensity at θ and D has been arbitrarily divided by the intensity at $\theta = 0$ and $D = D_0$. The curves are solid up to the point where the principal lobe has its minimum; the dashed portion of the curves represents the envelopes of the

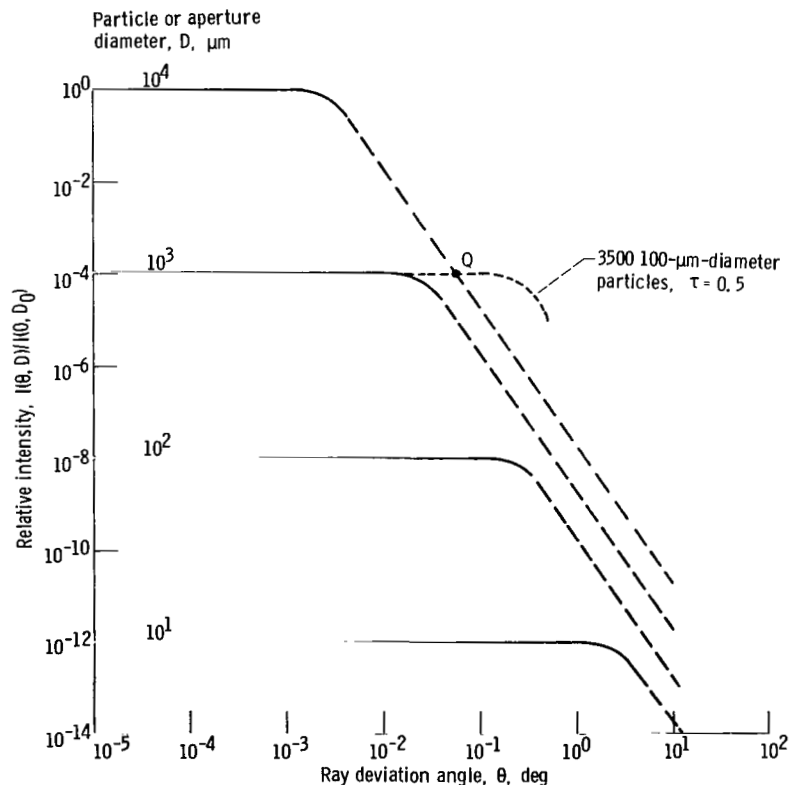


Figure 3. - Envelope of relative-intensity peaks of Fraunhofer diffraction. Wavelength of radiation, λ , 1 micrometer; particle diameter, D_0 , 10^4 micrometers at ray deviation angle $\theta = 0^\circ$.

second and higher lobes, and it is important when considering the possible effect of aperture diffraction. For $\alpha\theta > 1.84$, the intensity has been computed by equation (7). For $\alpha\theta < 1.84$, the intensity has been computed by equation (5). At $\alpha\theta = 1.84$, the two formulas yield the same numerical value within 2 percent.

To determine particle size solely from the ratio of two intensity measurements, one makes measurements in that part of the center scattering lobe which corresponds to the knee of the curves. For a single particle and a circular aperture, figure 3 shows that at the knee of the curve for a particle the ratio of intensities due to the aperture and to the particle is equal to the ratio of their respective diameters. This undesirably large ratio can be reduced by the following:

(1) A noncircular aperture can reduce the radiation intensity due to the aperture in one direction.

(2) Where the particle density is under the experimenter's control, many particles can be added to the test section to increase the intensity due to the particles and to reduce the intensity due to the aperture.

(3) Image processing by spatial filtering can reduce the intensity of light diffracted from the aperture.

Reduction of Influence of Test Section Aperture

The intensity of scattered light from the particles and from the aperture will be derived to show how to minimize the aperture-scattered light.

Apodization. - A noncircular aperture can redistribute the light intensity so that it is less in some directions. This modification, called aperture apodization, is treated in reference 12. Apodization can also be produced by modifying the radial intensity distribution over the aperture so that the intensity falls off with radius. This attenuation is to some degree inherent in the light from a laser source. For measurement applications this technique has the disadvantage of weighting the scattered light from a particle according to its position in the field of view.

Noncircular aperture. - To provide an example of aperture apodization, an elliptical aperture is considered. The ellipse has an axial width w and an axial height h . For convenience, define the ratios

$$\left. \begin{aligned} \alpha_w &= \frac{\pi w}{\lambda} \\ \alpha_h &= \frac{\pi h}{\lambda} \end{aligned} \right\} \quad (8)$$

The Fraunhofer equation for the ellipse gives the intensity along the w axis as

$$I(\theta_w) = \frac{H\lambda^2\alpha_w^2\alpha_h^2}{16\pi^2} \left[\frac{2J_1(\alpha_w\theta_w)}{\alpha_w\theta_w} \right]^2 \quad (9)$$

where H is the irradiance of a plane wave of radiation at the aperture.

Equation (6), with the cosine factor replaced by unity, is substituted in equation (9) to yield an approximate envelope of the intensity peaks along the w axis for $\alpha_w\theta_w > 1.84$. Along this envelope, for $\alpha_w\theta_w \geq 1.84$,

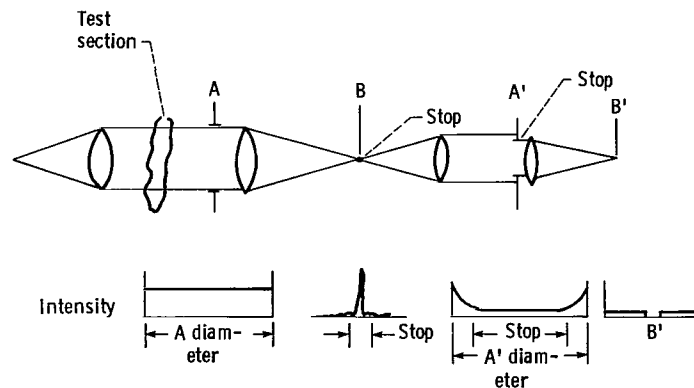
$$I(\theta_w) = \left(\frac{H\lambda^2}{16\pi^2} \right) \left(\frac{8\alpha_h^2}{\pi\theta_w^3\alpha_w} \right) \quad (10)$$

Elliptical apertures of constant area have $\alpha_w\alpha_h$ constant. Thus, an intensity reduction in equation (9) exists only when the quantity in square brackets is reduced. Equation (10) with $\alpha_w\alpha_h = \text{constant}$ thus shows that if an ellipse has a ratio $\alpha_w/\alpha_h = 10$ the intensity in the w-direction is reduced by a factor of $10\sqrt{10}$ and the intensity in the h-direction is increased by a factor $10\sqrt{10}$, relative to the intensity that would be produced by a circular aperture of the same area. An elliptical aperture may therefore be useful when its shape approximates the spray cross section to be measured. However, when the flux is measured with an annular aperture at the detector, there is no gain to using an elliptical test-section aperture unless the annular aperture can be masked so that radiation is received principally in two diagonally opposite quadrants. For particles of nonspherical shape, using a full annular aperture may be desirable in order to give an average-diameter measurement.

Spatial filtering. - Spatial filtering as described in references 13 and 14 requires reimaging the diffraction image plane in figure 1, as shown in figure 4(a). The test-section aperture A is reimaged to A', and the diffraction image plane B is reimaged to B'.

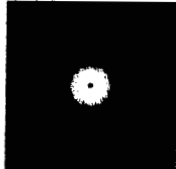
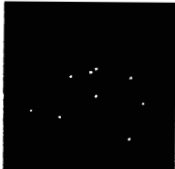

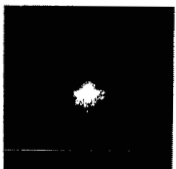
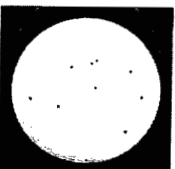

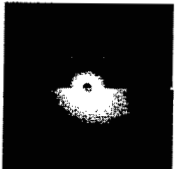
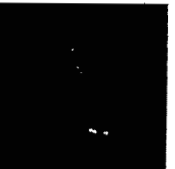

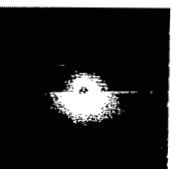


Let the spray particles be absent. A plane wave incident on A is focused at B. Most of the flux lies within the diameter of the first few rings of the Airy diffraction pattern when the optics are diffraction limited. A stop at B intercepts this flux. The flux that passed the stop was principally the flux diffracted near the edge of A where the angle of diffraction is greatest. The image of A at A' thus has the greatest intensity at the edge of A'. The stop at A' is smaller than the diameter A' and blocks most of the diffracted light. Thus, at the final image, B' is an image of the stop at B with a very low level of irradiance surrounding it. Reference 13 showed a reduction to less than 10^{-3} of the irradiance at B. The light diffracted by a particle in the test section at A is imaged at B and then reimaged at B' with no change of irradiance distribution except for a dark spot that is the image of the stop at B.

The photographs in figure 4(b) illustrate the effect of spatial filtering on the irradiance distributions with and without particles. The image



(a) Intensity distribution along optical path without particles in test section.

Figure 4. - Spatial filter.

Row	Image plane		
	B	A'	B'
1	Pinholes at test section, stop at B		
			
2	Dots at test section, no stops		
			
3	Clear test section, stop at B		
	No stop at A'	Spots due to lens defects	
4	Stop at A'		
5	Dots at test section, stop at B		
	No stop at A'	Spots due to film emulsion	
6	Stop at A'		

(b) Diffraction patterns to illustrate spatial filtering.

Figure 4. - Concluded.

planes of figure 4(a) are shown. Both pinholes and dots are represented. The pinholes provide a means of presenting the diffracted light produced by particles without the presence of diffracted light from the aperture. Where split images are shown, they represent the same image at two different exposures. The upper image, at shorter exposure, reveals more detail of the central lobe. The lower image, at longer exposure, reveals more detail of the outer, second lobe. Particles were simulated by a photograph on a glass plate of an array of holes in a metal sheet. The holes were located at randomly generated coordinates. Pinholes were produced by photographing a front-lighted metal sheet painted white. Dots were produced by photographing the sheet when it was backlighted. The final images on the photographic plate were made about 300 micrometers in diameter in order to produce a narrow-angle, high-intensity diffraction lobe and to reduce the effect of scattering by the optical elements or, in the case of dots, by the emulsion of the glass plate.

The first two rows of figure 4(b) show diffraction by pinholes and their inverse, dots. The pinholes give diffraction minima in accordance with equation (4). The dots give the same pattern, but it is masked by the much greater intensity of light due to aperture diffraction. This behavior is in agreement with the graph of figure 3: the ratio of aperture diameter to dot diameter is 50, and there are 9 particles. The intensity ratio on the sloping lines in figure 3 should be 50/9 which is sufficient to mask the minima of the diffraction pattern seen in the first row of figure 4(b).

The diffraction pattern from the particles can be recovered by intercepting the flux diffracted by the aperture. With no glass plate in the test section, the picture in row 3 shows that the aperture diffraction is concentrated in a narrow zone centered on the aperture edge. Lens defects produce some irregular spots. In row 4 the annular area has been intercepted by a stop placed at A'. The diffraction pattern at B' thereby has much lower intensity. With the glass plate in the test section, the fifth and sixth rows show the nine dots and many defects of the emulsion. The diffraction pattern at B' in row 6, compared with row 1, shows recovery of the diffraction minima, and a comparable intensity in the center diffraction lobe in which measurements are made.

Comparing rows 2 and 5 shows the effect of the stop at B on the image at B'. The light scattered by the optics between B and B' appears in row 2 at B' as several ghost images. This scattered light is eliminated in row 5 by the stop at B.

Aperture roughness. - It is desirable that the aperture have a smooth edge. If the test-section aperture has a rough edge, additional scattered radiation is produced. The result is extraneous scattered light. Serrated and ragged aperture edges were shown in reference 15 to produce undesired scattered light. It is therefore also important that the test section aperture is not vignetted by parts of the test section, such as the window frame.

Increasing the number of particles. - The intensity is proportional to the number of particles. As the number increases, more of the incident light is intercepted by the particles, and, assuming the particles are uniformly distributed over the aperture, the intensity of the aperture-diffracted light is reduced; thus, the transmission factor for the incident light becomes smaller.

When the number of particles is under the control of the experimenter, an increase in the number of particles may be advantageous. However, in the extreme, multiple scattering by the particles can distort the intensity profile. To avoid distortion, reference 4 suggests a transmission factor of not less than 0.2 for particles having 20-micrometer diameters. Smaller

particles have a larger scatter angle and require a larger limit to the transmission factor.

Since the transmission factor is related to the number of particles, it can indicate the gain in intensity when an unknown number N of particles is present. If N particles of diameter D_p are distributed in a test section of diameter D_b , the transmission factor (ref. 8) is

$$\tau(N) = \exp\left(\frac{-KN\pi D_p^2/4}{\pi D_b^2/4}\right) \quad (11)$$

where K is the scattering coefficient of a particle, equal to 2 for a particle larger than the wavelength. When $K = 2$, the flux intercepted by the cross-sectional area is scattered by reflection and refraction through the particle, and an equal amount of flux is Fraunhofer diffracted on passing outside the particle. Thus, the diffracted radiation from N particles is equal to one-half the flux removed from the beam, which is a fraction $[1 - \tau(N)]/2$ of the incident light. The gain over the light intensity from one particle is thus

$$\frac{1 - \tau(N)}{1 - \tau(1)} = \frac{1}{2}[(1 - \tau(N))\left(\frac{D_b}{D_p}\right)^2] \quad (12)$$

where $\tau(1)$ is near unity so that the first two terms of the series approximation of τ are adequate to replace the denominator of equation (12), and K has been set equal to 2.

The intensity produced by the test section aperture is reduced by the transmission factor $\tau(N)$. Thus, the overall effective gain in intensity is the gain in equation (12) times $1/\tau(N)$:

$$G = \frac{[1 - \tau(N)]}{2\tau(N)}\left(\frac{D_b}{D_p}\right)^2 \quad (13)$$

When $\tau = 0.5$, the factor $(1 - \tau)/\tau = 1$. For example, if $\tau = 0.5$, the beam diameter is 1 cm = 10^4 micrometers, and the particle diameter is 100 micrometers, there are 3500 particles and equation (13) gives an intensity gain G of 10^4 . The relative intensity distribution for these conditions is shown as a dotted line in figure 3. At point Q, the relative intensities of radiation from the particle and from the aperture are equal to each other.

Interference of Scattered Light

The curves of figure 2 assume that the light from many particles is the sum of the light from individual particles. The actual intensity is dependent on the spatial distribution of the particles and the resulting interference of light scattered from several particles. This interference is most pronounced with a monodispersion of a small number of particles. For example, see figure 4(b), row 1. The interference when there are particle arrays is analyzed in references 16 to 18. When the number of particles is large, the effect of interference on the pattern becomes negligible. How-

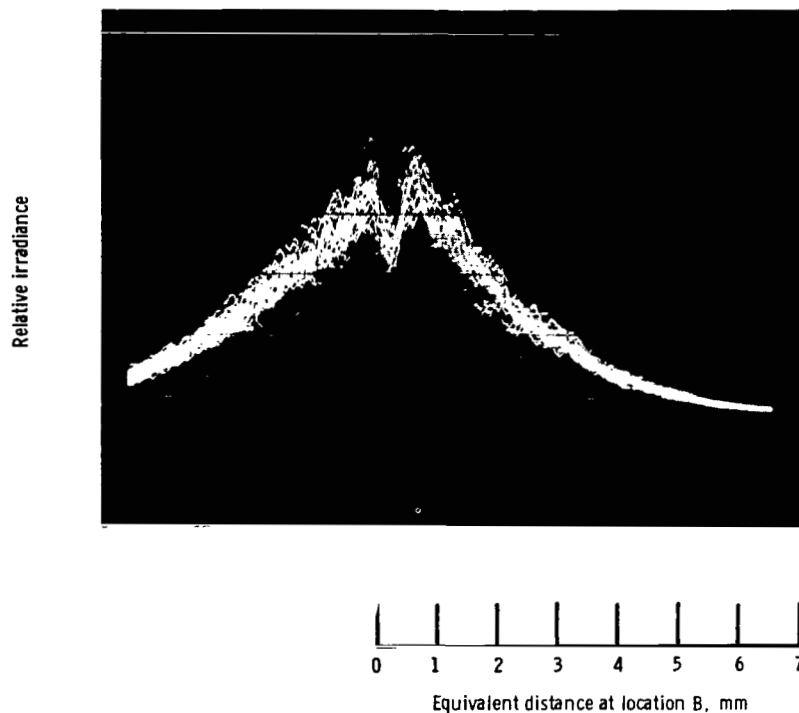


Figure 5. - Irradiance distribution along axis of image plane, showing 15 repetitive scans of moving 50-micrometer diameter particles. Scanning aperture, 0.4-millimeter diameter; axial stop, 0.4-millimeter diameter.

ever, the speckle caused by laser light is superimposed on the average intensity distribution. This speckle is also shown in figure 4(b), row 1.

To illustrate the effect of speckle, 50-micrometer-diameter particles of latex were immersed in water and stirred to produce a slowly changing particle distribution. The intensity distribution was recorded along the path of a scanning aperture for a number of repetitive scans. The record, in figure 5, shows that each curve has a substantial fluctuation about a mean of all curves, analogous to a record of noise superposed on a desired signal. It is necessary to minimize the noise and to recover the signal.

Techniques that would reduce the intensity fluctuation in some circumstances are the following:

- (1) Integration over the spectral bandwidth of a nonmonochromatic source to sum independent monochromatic intensity distributions
- (2) Integration over an annular ring
- (3) Integration over time, as evident from figure 5

Integration (1) is not possible with a laser source, which is generally used because it can deliver a much greater flux to the detector from a smaller source diameter. A helium-neon laser has 10^5 greater brightness than a 2800 K tungsten lamp at a center wavelength of 0.65 micrometer and a bandwidth of 0.1 micrometer.

Integration (2) can be done for a small number of rings as applied to the method of references 1 to 3. It is not feasible for a scanning system.

Integration (3) is easily done by a low-pass signal filter for the method of references 1 to 3. It is not possible with a simple scanning

aperture and single detector. Time integration can be done by using a charge-coupled linear detector array or a television camera. However, these detectors are limited in dynamic range so that it may be difficult to use them when there is a wide variation in intensity of radiation at the detector.

Gas Density Gradients

The collimated beam in the test section is refracted when there are gas temperature gradients or turbulence. This refraction broadens the irradiance distribution at the image point of the objective lens. Point-image broadening by atmospheric turbulence has been extensively studied for its effect on astronomical telescope resolution (ref. 19). Correction for point-image broadening caused by laboratory generated turbulence was studied in reference 20. These applications were concerned with the central part of the point image that contains most of the total flux; the low-level irradiance farther away from the center was not significant.

For particle sizing where low-level irradiance is significant, a test was made with hot-air turbulence produced by an electric heat gun that blew air at a velocity of 4 meters per second and a temperature of 250° C above ambient over a 3-centimeter-deep test section. The relative irradiance distribution from a point source at a 0.63-micrometer wavelength is shown in figure 6 before and after the turbulence was generated. The relative ir-

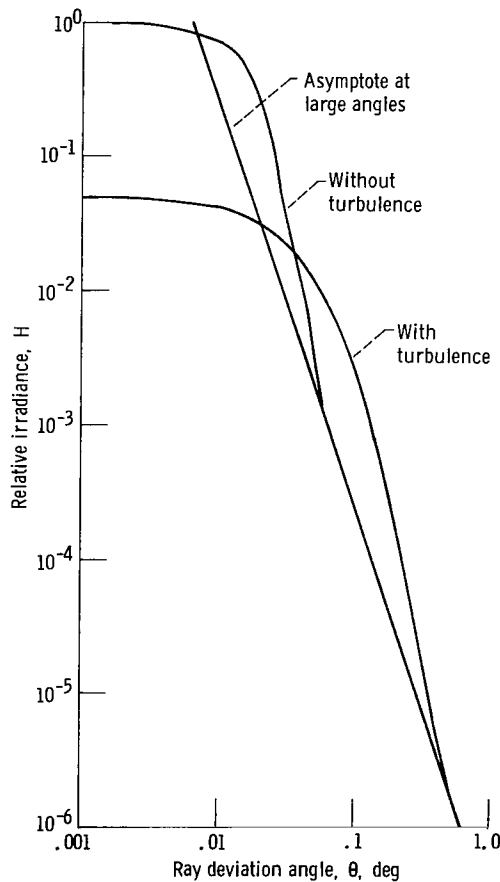


Figure 6. - Image irradiance distribution with and without hot-air turbulence in test section.

radiance distribution without turbulence is in agreement with figure 3, which shows a reduction with the cube of beam spread angle θ at large angles. At small angles near the maximum irradiance, broadening is increased in proportion to the spread functions of lens aberration and detector aperture diameter. When turbulence is added, broadening at small angles is further increased by the presence of the turbulence spread function. At large angles, the irradiance again approaches a dropoff with the cube of the angle.

The turbulence also broadens the irradiance distribution caused by particle diffraction. This broadening can be estimated and corrected for. For example, figure 2 shows that, at a wavelength of 0.65 micrometer, a particle with a 100-micrometer diameter has an irradiance distribution whose half-maximum width occurs at a ray deviation angle $\theta_{1/2}$ of 0.170° . The experimental curve for the turbulent condition in figure 6 shows that the half-maximum occurs at a ray deviation angle of 0.028° . This represents the broadening that occurred in this experiment. The resultant value of $\theta_{1/2}$ is the square root of the sum of the squares of the two angles, or 0.172° , which represents a 1-percent error.

To apply spatial filtering with turbulence present, the stop at the focus of the objective lens must be increased in diameter to intercept most of the flux at the broadened image point so that there is no sharp increase of radiation at the periphery of the image of the stop.

Extraneous Light

In experiments, the scattered light to be measured is combined with extraneous light from the instrument components and from the test section. For example, the instrument with perfect optics and a point source has the collimated beam diffracted by the test section aperture. This diffracted light is relatively stronger at small scatter angles, as was shown in figure 3. However, scattering is also produced by optical surfaces that can become dirty during the course of an experiment. Test section turbulence was shown in figure 6 also to increase the extraneous light at small scatter angles.

Response to extraneous light was eliminated in reference 9 by measurement with two known concentrations of particles, and in reference 10 with a laser heterodyne apparatus that responded only to particles in motion. It was shown that extraneous light was most likely to be a problem at small scatter angles. Thus, it is desirable to use a measurement method that does not require measurement of scattered light at small angles. The two-angle methods can have this desirable property.

Comparison of Fraunhofer Diffraction and Mie Theory

For particle sizing, the angular distribution of scattered light is approximated by Fraunhofer diffraction. An error is caused by the difference from the exact distribution given by the Mie theory. In reference 21 the error for a monodispersion with two fixed-angle measurements was determined using the method of reference 1. In reference 22 the Fraunhofer equation was better modified to approximate the Mie theory for application to particle size distribution.

An explicit comparison of Fraunhofer and Mie scattering is given herein for a better understanding of some limits to accuracy and the effect of a polydispersion. Figure 7 shows a smoothed curve of the maximum relative intensity (at $\theta = 0$) as given by Mie's theory and the width, $2\theta_{1/2}$, at one-half the maximum intensity for water particles in air. The relative

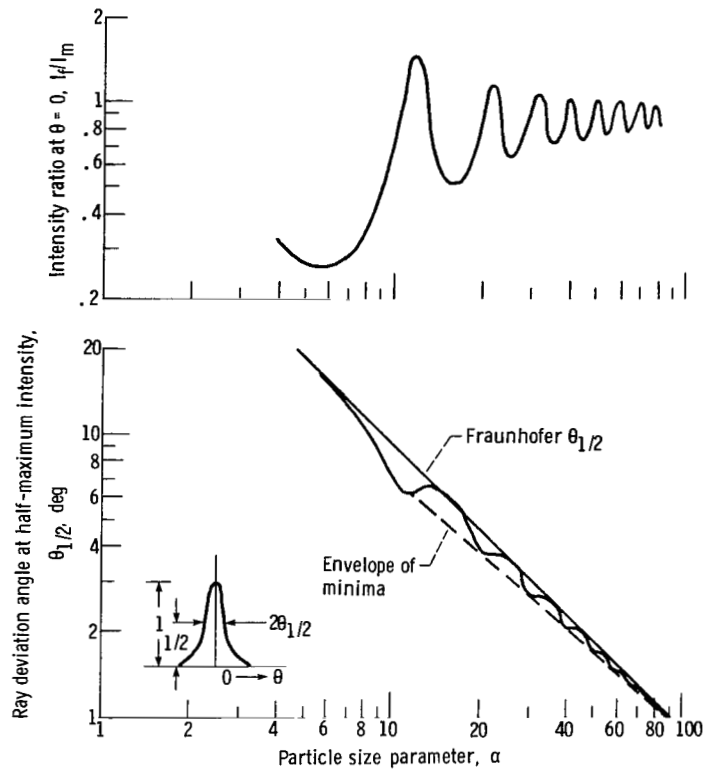


Figure 7. - Comparison of Fraunhofer diffraction with Mie formula. Refraction index, 1.33.

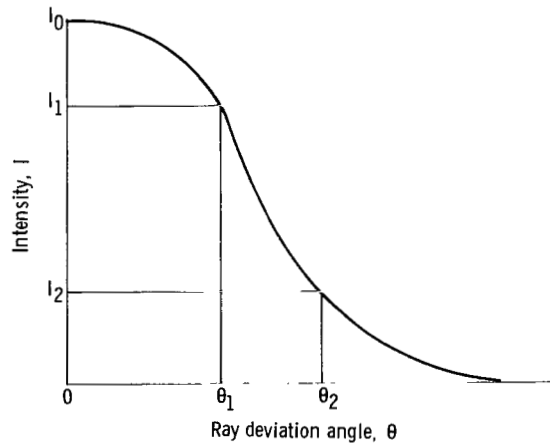


Figure 8. - Two-angle measurement.

intensity, as presented, is the intensity as computed by the Fraunhofer formula divided by the intensity as computed by the Mie theory. The half-maximum width for the Mie computation was determined by interpolating between tabulated values of intensity distribution with θ for each given α . The difference between the two curves for θ at half-maximum is -22 percent near $\alpha = 10$ (approximately 2- μm particle diameter at $\lambda = 0.63 \mu\text{m}$) and less everywhere else. A polydispersion shows smaller differences because the Mie curves are averaged over the diameter distribution.

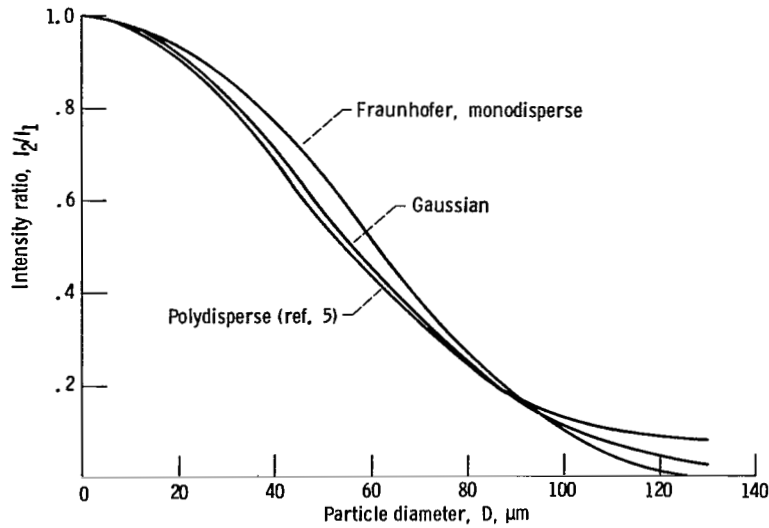


Figure 9. - Particle diameter by method 1. Ray deviation angles, $\theta_1 = 0.003$ radian, $\theta_2 = 0.006$ radian; wavelength of radiation, λ , 0.6328 micrometer.

MEASUREMENT OF SCATTERED LIGHT AT TWO ANGLES

Description of the Two Methods

In figure 8 the light scattered by particles has intensities I_0 , I_1 , and I_2 at angles $\theta = 0$, θ_1 , and θ_2 . It is assumed that there is no extraneous light present. Using the Gaussian approximation of scattering (fig. 2) gives the ratio of intensities at two angles as

$$I_2/I_1 = \exp[-(0.57\pi D/\lambda)^2(\theta_2^2 - \theta_1^2)] \quad (14)$$

Solving for the diameter gives

$$D^2 = -(\lambda/0.57\pi)^2 \ln(I_2/I_1)/(\theta_2^2 - \theta_1^2) \quad (15)$$

Equation (15) is a basis for both methods.

Method 1: Measurements at fixed angles θ_1 and θ_2 (refs. 1 to 3). - In this method, the diameter D in equation (15) is obtained from the measurement of I_2/I_1 . Equation (15) is plotted in figure 9 for a typical set of values of θ_1 , θ_2 , and λ . Curves are shown for a monodispersion by Fraunhofer diffraction, a polydispersion by the data of reference 5, and the Gaussian approximation. In all cases the usable range of D is limited at large and small values by the inaccuracy of the intensity measurement. When the diameter is small, the fixed angles θ_1 and θ_2 are both smaller than they should be to minimize extraneous light. This disadvantage of small angles can be reduced by measuring at more than two fixed angles and then by selecting the most favorable pair for computation.

Method 2: Measurement of θ_2 at constant intensity ratio I_2/I_1 and fixed angle θ_1 (ref. 4). - With this method the diameter D in equation (15) depends on the measurement of θ_2 . In this method, the scanning angle is increased continuously from an initial value θ_1 . Intensity I_1 is first

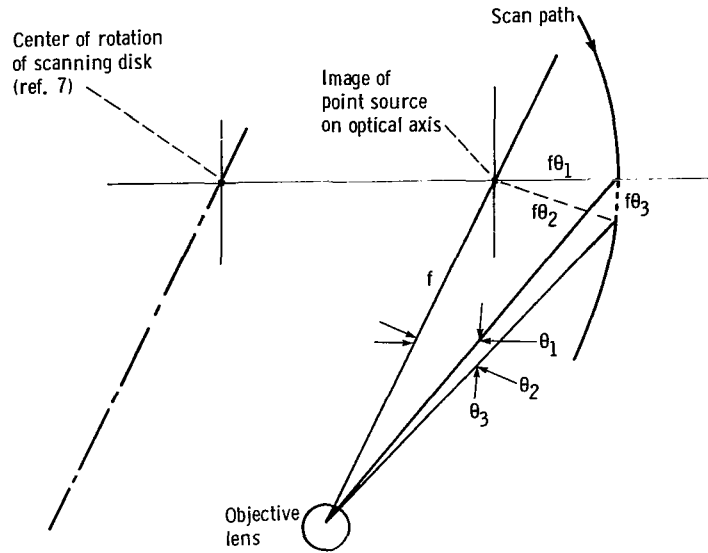


Figure 10. - Off-axis scanning in image plane by method 2.

measured at a fixed angle θ_1 , and then, as scanning continues, the intensity drops until it reaches a preset ratio I_2/I_1 . At this time, the angle θ_2 is measured.

A scanning path, as used in reference 7, is shown in figure 10. The path is off the optical axis by a distance $f\theta_1$ subtending a fixed angle θ_1 from the objective lens. The measured angle θ_3 has the relationship

$$\theta_3^2 = \theta_2^2 - \theta_1^2 \quad (16)$$

Substituting equation (16) in equation (15) gives

$$D^2 = -\ln(I_2/I_1)/C^2\theta_3^2 \quad (17)$$

where $C = 0.57\pi/\lambda$ and $I_2 < I_1$, so that D depends only on θ_3 and is independent of θ_1 . Angle θ_1 is usually set, by adjustment of the off-axis distance of the scanning path, so as to minimize the effects of extraneous light.

Method 2 has the disadvantage of not integrating the intensity over an annular ring as may be done with method 1. Since there is also the disadvantage that I_1 and I_2 are not measured simultaneously, there is a fluctuation in the intensity ratio on successive scans when I_1 and I_2 are changing. Time integration can be made of the processed signal that indicates θ_3 . In practice, a low-pass filter time constant of 1 second is adequate to produce an adequately steady reading of the angle.

Accuracy of the Two Methods

Differentiating equation (15) gives the error in D caused by error in intensity measurement:

$$\frac{dD}{D} = \frac{1}{2 \ln(I_2/I_1)} \left(\frac{dI_2}{I_2 I_1} - \frac{dI_1}{I_2 I_1} \right) \quad (18)$$

when θ_1 and θ_2 are measured with negligible error. Because the various sources of extraneous light are independent of I , we assume that the random error dI of intensity is constant and not dependent on I , and that the variances $(dI_1)^2$ and $(dI_2)^2$ are each equal to $(dI)^2$. Then equation (18) can be written as

$$\left| \frac{dD/D}{dI/I_0} \right| = \left[\frac{\left(\frac{I_0}{I_2} \right)^2 + \left(\frac{I_0}{I_1} \right)^2}{2 |\ln(I_2/I_1)|} \right]^{1/2} \quad (19)$$

Equation (19) is written for method 1 in terms of D and the instrument constants θ_1 and θ_2 as

$$\left| \frac{dD/D}{dI/I_0} \right| = \frac{\left[\frac{2(CD\theta_2)^2}{e} + \frac{2(CD\theta_1)^2}{e} \right]^{1/2}}{2C^2D^2 |\theta_2^2 - \theta_1^2|} \quad (20)$$

where $C \equiv 0.57\pi/\lambda$ and I_0 is the intensity at $\theta = 0$.

Equation (19) is written for method 2 in terms of D and the instrument constants θ_1 and I_2/I_1 as

$$\left| \frac{dD/D}{dI/I_0} \right| = - \frac{\left[1 + (I_1/I_2)^2 \right]^{1/2} (CD\theta_1)^2}{2 |\ln(I_2/I_1)|} \quad (21)$$

Equation (20) for method 1 is plotted in figure 11 for $\theta_2/\theta_1 = 1.5, 2$, and 3 with $\theta_1 = 0.003$; and for $\theta_2/\theta_1 = 3$ with $\theta_1 = 0.0015$. The choice of the

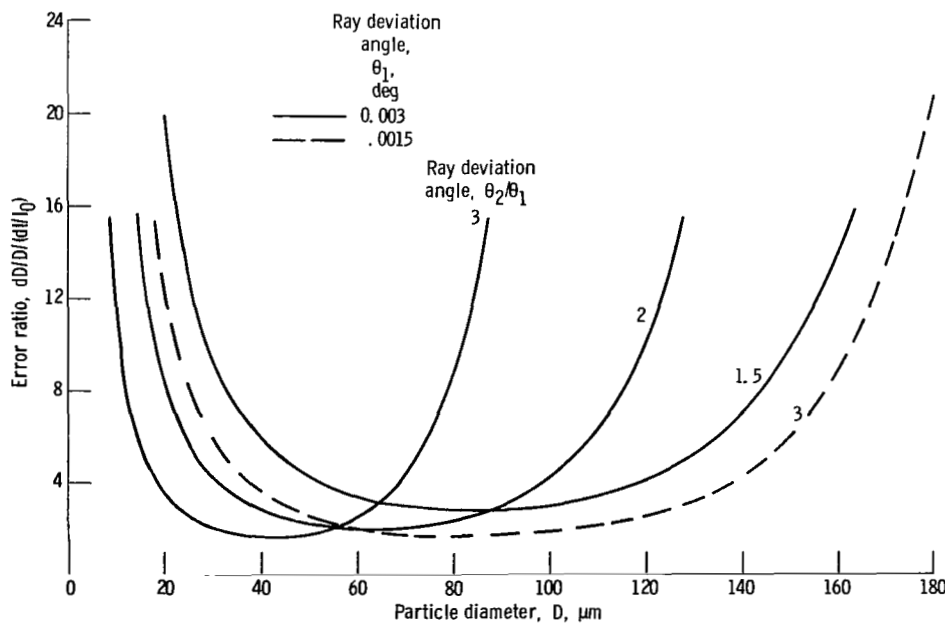


Figure 11. - Error ratio of method 1 (eq. (20)). Wavelength of radiation, λ , 0.6328 micrometer.

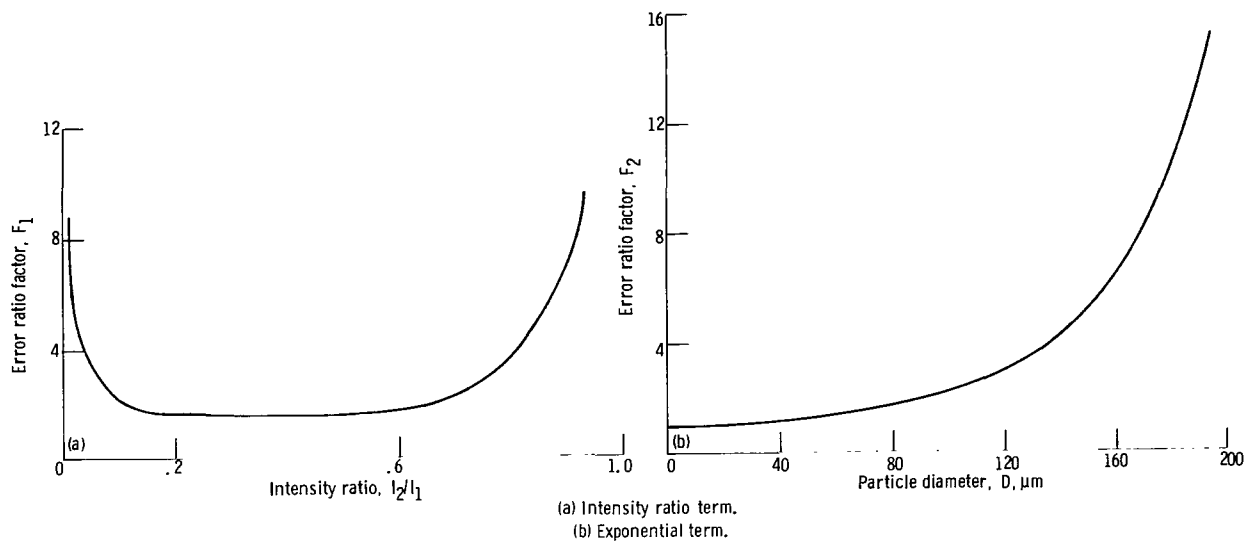


Figure 12. - Error ratio factors for method 2 (eq. (21)). Ray deviation angle, θ_1 , 0.003 radian; wavelength of radiation, λ , 0.6328 micrometer; error ratio, $F_1 F_2 = |dD/D| / |dI/I_0|$.

values of θ_1 and θ_2/θ_1 depends on the range of particle diameters that are of principal interest. Acceptably small inaccuracy in diameter measurement is more likely to be achieved where the error ratio $|(dD/D)/(dI/I_0)|$ is small. However, figure 11 presents information only on the magnitude of the error ratio. There are also other considerations; for example, the choice of a smaller θ_1 would result in an increase in the amount of extraneous light and thereby an increase in the magnitude of dI/I_0 .

Equation (21) for method 2 has the independent parameters I_2/I_1 and θ_1 and the independent variable D . Thus, the error ratio may be represented as the product of two factors, F_1 and F_2 - the first dependent solely on I_2/I_1 , the second dependent on D and θ_1 . These factors are plotted separately in figure 12. In figure 12(a), the factor F_1 has a broad minimum when the intensity ratio lies between 0.2 and 0.6. In figure 12(b), the factor F_2 places an upper limit on the largest particle diameter that may be measured reliably. At the large-diameter end, the resultant error ratio is comparable to that of method 1 with $\theta_1 = 0.003$ and $\theta_2/\theta_1 = 1.5$. At the small-diameter end, method 2 is superior.

For both methods the largest acceptable value of angle θ_1 is usually determined by the largest particle diameter to be measured reliably. If one arbitrarily chooses $\theta_1 = 0.003$ and the criterion that the error ratio be less than 4, figures 11 and 12 show that the maximum particle diameter that may be measured reliably is as follows:

(1) For method 1,

70 μm if $\theta_2/\theta_1 = 3$
 100 μm if $\theta_2/\theta_1 = 2$
 120 μm if $\theta_2/\theta_1 = 1.5$

(2) For method 2,

110 μm if $I_2/I_1 = 0.5$

A generalization of these conclusions is derivable from the fact that equation (15) is really a statement about the beam spread parameter $\pi D\theta/\lambda$ so that in the present analysis, the product $D\theta$ is constant. Hence, under the criterion that the error ratio be less than 4, it may be concluded that if D_{max} is the maximum particle diameter that may be measured reliably it is given by the following:

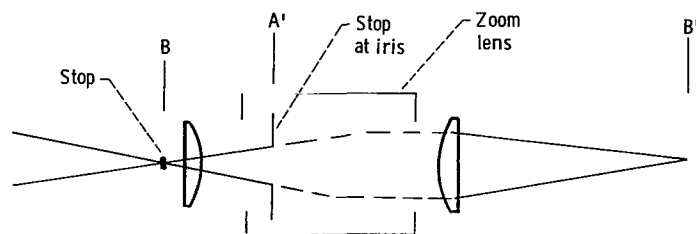


Figure 13. - Zoom lens as part of image relay optics.

(1) For method 1,

$$\begin{aligned}\theta_1 D_{\max} &= 0.21 \mu\text{m} \text{ if } \theta_2/\theta_1 = 3 \\ \theta_1 D_{\max} &= 0.30 \mu\text{m} \text{ if } \theta_2/\theta_1 = 2 \\ \theta_1 D_{\max} &= 0.36 \mu\text{m} \text{ if } \theta_2/\theta_1 = 1.5\end{aligned}$$

(2) For method 2,

$$\theta_1 D_{\max} = 0.33 \mu\text{m} \text{ if } I_2/I_1 = 0.5$$

These results show that both methods are comparable in their criteria for the largest acceptable value of θ_1 .

Instrument with Zoom Lens

Using of a zoom lens may serve to adjust the angle θ_1 to be more nearly optimum for any particular particle diameter. The theory and description of zoom lenses are given in references 23 to 25. Commercially available lenses have zoom ratios of 3 to 10. Such a lens added to the imaging portion of the optical system of figure 4(a) is shown in figure 13. The zoom lens is positioned for a reversed direction of light, so its image plane is at the stop B. The zoom lens iris becomes the stop A' for spatial filtering. This iris is stationary in the zoom lens because the movable lenses are to the right of the iris.

The spatial filter stop at B preceding the relay optics is required to prevent light scattering by the zoom lens. The stop at A' is not required, but it may be desirable. Then the only light incident on the zoom lens and scattered by it is the light already scattered from particles. The zoom lens varies the effective focal length of the objective lens and thus the image size at the detector. As a result, (1) the angle of measurement θ_1 may be set at an optimum value for the particle size being measured, and (2) the flux received by the detector that ordinarily varies with particle size as D^{-4} will now vary much less strongly as D^{-2} .

Because the size of the detector at B' is fixed, the zoom lens varies the conjugate image at B. The biggest acceptable image at B is equal to the zoom lens nominal image size at its longest focal length. As the focal length is reduced, the image at B is reduced, thus completely avoiding vignetting by the lens if vignetting is zero for the longest focal length. Vignetting at the longest focal length may be avoided by limiting the aperture ratio of the lens with its iris.

In general, the commercial zoom lens has more flexible performance than needed in this application. Since in this application the object distance is fixed and the field of view is small and constant, rather than increasing as the focal length is reduced, vignetting and wide-angle aberration are avoided. Also, the use of monochromatic light eliminates chromatic aberration.

COMPARISON OF THE TWO METHODS

The two methods are compared herein for the following characteristics:

(1) Frequency response. Method 1 measures two intensities simultaneously and continuously. Method 2 is limited to periods that are long compared to the time of a scanning period.

(2) Real-time output of steady-state input. Method 1 is sufficiently linear over a limited diameter range to be capable of simple signal processing, which gives the ratio of two signals before correcting for extraneous light. Correcting for extraneous light is done by subtracting readings at the two angles with and without spray, and then calculating the ratio. Method 2 is linear over a large diameter range and is capable of simple signal processing before correcting for extraneous light. Correcting for extraneous light is nonlinear. It is done by computation or by a graph using readings with and without spray.

(3) Adjustment of instrument for optimum measurement angle θ_1 . Method 1 requires multiple detectors or a zoom lens. Method 2 requires adjusting the distance between the optical axis and the scanning path, or a zoom lens.

(4) Integration of laser speckle and spray fluctuation. Method 1 is better adapted to spatial and temporal integration at the detector. Both methods can integrate the processed signal with some loss of frequency response.

Both methods have the limitations set by aperture diffraction, interference, and refraction that were presented in the section Light Scattering Analysis. These limitations appear to be more significant than the other differences between the two types of instrument.

CONCLUSIONS

The light scattered by particles was shown to be affected by extraneous light from a number of causes:

- (1) Diffraction by the test section aperture
- (2) Speckle caused by a laser light source
- (3) Refraction due to gas density gradients in the test section
- (4) Dirty test section windows

Methods to minimize the extraneous light were presented for application to instrument design. In particular, optimum values of the operating parameters were determined for two methods that compare intensities at two angles of measurement in order to deduce particle diameter.

Lewis Research Center
National Aeronautics and Space Administration
Cleveland, Ohio January 12, 1983

REFERENCES

1. Hodkinson, J. R.: Particle Sizing by Means of the Forward Scattering Lobe. Appl. Opt., vol. 5, no. 5, May 1966, pp. 839-844.

2. Mullaney, P. F.; and Dean, P. N.: Cell Sizing: A Small-Angle Light-Scattering Method for Sizing Particles of Low Relative Refractive Index. *Appl. Opt.*, vol. 8, no. 11, Nov. 1969, pp. 2361-2362.
3. Gravatt, C. C., Jr.: Real Time Measurement of the Size Distribution of Particulate Matter by a Light Scattering Method. *J. Air Pollut. Control Assoc.*, vol. 23, no. 12, Dec. 1973, pp. 1035-1038.
4. Dobbins, R. A.; Crocco, L.; and Glassman, I.: Measurement of Mean Particle Sizes of Sprays from Diffractively Scattered Light. *AIAA J.*, vol. 1, no. 8, Aug. 1963, pp. 1882-1886.
5. Roberts, J. H.; and Webb, M. J.: Measurement of Droplet Size for Wide Range Particle Distributions. *AIAA J.*, vol. 2, no. 3, Mar. 1964, pp. 583-585.
6. Dieck, R. H.; and Roberts, R. L.: The Determination of the Sauter Mean Droplet Diameter in Fuel Nozzle Sprays. *Appl. Opt.*, vol. 9, no. 9, Sept. 1970, pp. 2007-2014.
7. Buchele, D. R.: Scanning Radiometer for Measurement of Forward-Scattered Light to Determine Mean Diameter of Spray Particles. *NASA TM X-3454*, Nov. 1976.
8. Gumprecht, R. O.; and Sliepcevich, C. M.: Scattering of Light by Large Spherical Particles. *J. Phys. Chem.*, vol. 57, no. 1, Jan. 1953, pp. 90-95.
9. Spinrad, R. W.; Zaneveld, J. R. V.; and Pak, H.: Volume Scattering Function of Suspended Particulate Matter at Near-Forward Angles: A Comparison of Experimental and Theoretical Values. *Appl. Opt.*, vol. 17, no. 7, Apr. 1978, pp. 1125-1130.
10. Hard, S.; and Nilsson, O.: Laser Heterodyne Apparatus for Measuring Small Angle Scattering From Particles. *Appl. Opt.*, vol. 18, no. 17, Sept. 1979, pp. 3018-3026.
11. Hildebrand, F. B.: *Advanced Calculus for Engineers*. Prentice-Hall, Inc., 1949.
12. Jacquinet, P.; and Roizen-Dossier, B.: Apodisation. *Progress in Optics*, vol. III, E. Wolf, ed., North-Holland Publ. Co., 1964, pp. 29-186.
13. Blodgett, J. A.; and Easton, R. L., Jr.: Two-Stage Spatial Filtering for Diffraction Pattern Analysis. *Appl. Opt.*, vol. 20, no. 6, Mar. 1981, pp. 1050-1055.
14. Hutzler, P. J. S.: Spatical Frequency Filtering and its Application to Microscopy. *Appl. Opt.*, vol. 16, no. 8, Aug. 1977, pp. 2264-2272.
15. George, N.; and Morris, G. M.: Diffraction by Serrated Apertures. *J. Opt. Soc. Am.*, vol. 70, no. 1, Jan. 1980, pp. 6-17.
16. Stone, J. M.: *Radiation and Optics*. McGraw-Hill Book Co., Inc., 1963.
17. Lipson, S. O.; and Lipson, H.: *Optical Physics*. Cambridge Univ. Press, 1969.
18. Williams, C. S.; and Becklund, O. A.: *Optics: A Short Course for Engineers and Scientists*. John Wiley and Sons, Inc., 1972.
19. Kuiper, G. P.; and Middlehurst, B. M.: *Telescopes*. Univ. of Chicago Press, 1960.
20. McGlamery, B. L.: Restoration of Turbulence-Degraded Images. *J. Opt. Soc. Am.*, vol. 57, no. 3, Mar. 1967, pp. 293-297.
21. Boron, S.; and Waldie, B.: Particle Sizing by Forward Lobe Scattered Intensity-Ratio Technique: Errors Introduced by Applying Diffraction Theory in the Mie Regime. *Appl. Opt.*, vol. 17, no. 10, May 15, 1978, pp. 1644-1648.

22. Fymat, A. L.; and Mease, K. D.: Mie Forward Scattering: Improving Semiempirical Approximation with Application to Particle Size Distribution Inversion. Appl. Opt., vol. 20, no. 2, Jan. 15, 1981, pp. 194-198.
23. Bergstern, L.; and Motz, L.: Four-Component Optically Compensated Varifocal System. J. Opt. Soc. Am., vol. 52, no. 4, Apr. 1962, pp. 376-388.
24. Kingslake, R.: Desing of Zoom Lenses. Applied Optics and Optical Engineering, vol. III, R. Kingslake, ed., Academic Press, 1965, pp. 34-38.
25. Cook, G. H.: Variable Focal Length and Zoom Objectives. Applied Optics and Optical Engineering, vol. III, R. Kingslake, ed., Academic Press, 1965. pp. 132-139.

1. Report No. NASA TP-2156	2. Government Accession No.	3. Recipient's Catalog No.	
4. Title and Subtitle PARTICLE SIZING BY MEASUREMENT OF FORWARD-SCATTERED LIGHT AT TWO ANGLES		5. Report Date May 1983	
		6. Performing Organization Code 505-32-82	
7. Author(s) Donald R. Buchele		8. Performing Organization Report No. E-1179	
		10. Work Unit No.	
9. Performing Organization Name and Address National Aeronautics and Space Administration Lewis Research Center Cleveland, Ohio 44135		11. Contract or Grant No.	
		13. Type of Report and Period Covered Technical Paper	
12. Sponsoring Agency Name and Address National Aeronautics and Space Administration Washington, D. C. 20546		14. Sponsoring Agency Code	
15. Supplementary Notes			
16. Abstract Fundamental and practical limitations to particle sizing by measurement of forward-scattered light are presented. Methods to minimize the limitations are described. Two types of instrument are compared.			
17. Key Words (Suggested by Author(s)) Scattered light; Particle sizing; Fuel spray		18. Distribution Statement Unclassified - unlimited STAR Category 07	
19. Security Classif. (of this report) Unclassified	20. Security Classif. (of this page) Unclassified	21. No. of Pages 26	22. Price* A03

National Aeronautics and
Space Administration

THIRD-CLASS BULK RATE

Postage and Fees Paid
National Aeronautics and
Space Administration
NASA-451



Washington, D.C.
20546

Official Business

Penalty for Private Use, \$300

5 1 10, A, 830517 S00903DS
DEPT OF THE AIR FORCE
AF WEAPONS LABORATORY
ATTN: TECHNICAL LIBRARY (SUL)
KIRTLAND AFB NM 87117

NASA

POSTMASTER: If Undeliverable (Section 158
Postal Manual) Do Not Return
